Cell Reports

Article

Protein phosphatase 1 acts as a RIF1 effector to suppress DSB resection prior to Shieldin action

Graphical abstract

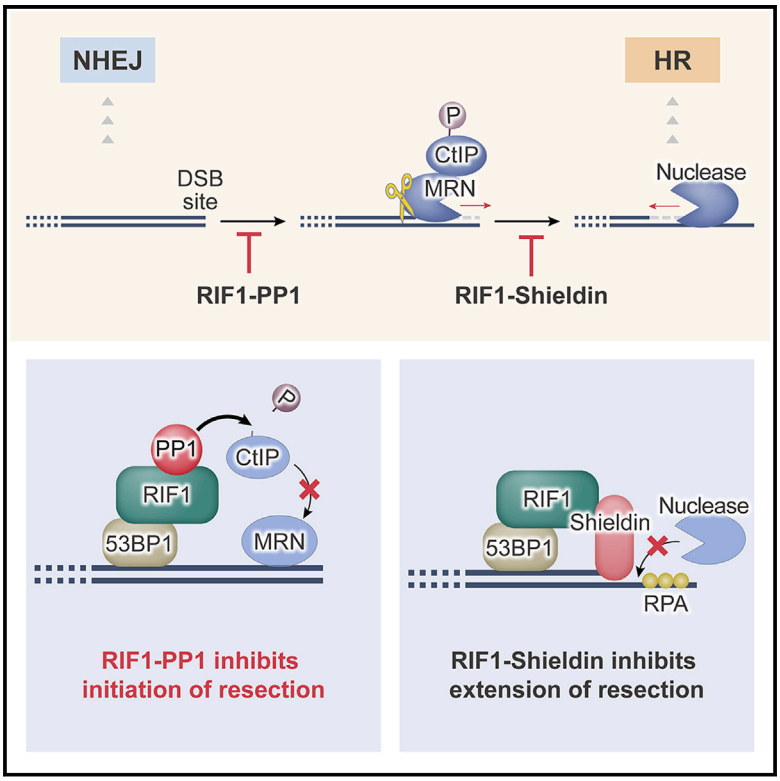

Highlights

- PP1 acts as a RIF1 effector distinct from shieldin in DNA damage repair
- PP1 accumulates at damage sites dependent on RIF1 and 53BP1
- RIF1-PP1 suppresses assembly of CtIP damage foci to limit resection initiation by MRN
- PP1 and shieldin cooperate to prevent precocious HR in the early damage response

Authors

Shin-Ya Isobe, Shin-ichiro Hiraga, Koji Nagao, Hiroyuki Sasanuma, Anne D. Donaldson, Chikashi Obuse

Correspondence

obuse@bio.sci.osaka-u.ac.jp

In brief

Isobe et al. show that PP1 acts as a RIF1 effector distinct from shieldin in DNA damage repair. RIF1-PP1 inhibits the initiation of resection by CtIP-MRN prior to shieldin action. PP1 and shieldin, as RIF1 effectors, cooperate to suppress premature homologous recombination in the early stage of the damage response.

Isobe et al., 2021, Cell Reports *36*, 109383
July 13, 2021
https://doi.org/10.1016/j.celrep.2021.109383

CellPress

Cell Reports

CellPress
OPEN ACCESS

Article

Protein phosphatase 1 acts as a RIF1 effector to suppress DSB resection prior to Shieldin action

Shin-Ya Isobe,[1] Shin-ichiro Hiraga,[2] Koji Nagao,[1] Hiroyuki Sasanuma,[3] Anne D. Donaldson,[2] and Chikashi Obuse[1,4,*]
[1]Department of Biological Sciences, Graduate School of Science, Osaka University, 1-1 Machikaneyama-Cho, Toyonaka, Osaka 560-0043, Japan
[2]Institute of Medical Sciences, School of Medicine, Medical Sciences & Nutrition, University of Aberdeen, Aberdeen AB25 2ZD, UK
[3]Department of Genome Medicine, Tokyo Metropolitan Institute of Medical Science, Tokyo, Japan
[4]Lead contact
*Correspondence: obuse@bio.sci.osaka-u.ac.jp
https://doi.org/10.1016/j.celrep.2021.109383

SUMMARY

DNA double-strand breaks (DSBs) are repaired mainly by non-homologous end joining (NHEJ) or homologous recombination (HR). RIF1 negatively regulates resection through the effector Shieldin, which associates with a short 3′ single-stranded DNA (ssDNA) overhang by the MRN (MRE11-RAD50-NBS1) complex, to prevent further resection and HR repair. In this study, we show that RIF1, but not Shieldin, inhibits the accumulation of CtIP at DSB sites immediately after damage, suggesting that RIF1 has another effector besides Shieldin. We find that protein phosphatase 1 (PP1), a known RIF1 effector in replication, localizes at damage sites dependent on RIF1, where it suppresses downstream CtIP accumulation and limits the resection by the MRN complex. PP1 therefore acts as a RIF1 effector distinct from Shieldin. Furthermore, PP1 deficiency in the context of Shieldin depletion elevates HR immediately after irradiation. We conclude that PP1 inhibits resection before the action of Shieldin to prevent precocious HR in the early phase of the damage response.

INTRODUCTION

Double-strand breaks (DSBs) are known to be repaired mainly by non-homologous end joining (NHEJ) or homologous recombination (HR), and failure of these repair mechanisms causes cell death, chromosome rearrangement, and carcinogenesis (Symington and Gautier, 2011). NHEJ is active throughout the cell cycle (Shibata and Jeggo, 2020; Symington and Gautier, 2011) and is used for programmed DSB repairs, such as V(D)J recombination and immunoglobulin class switching (Di Virgilio et al., 2013; Difilippantonio et al., 2008; Zimmermann and de Lange, 2014). Alternatively, HR is activated during S and G_2 phases and is initiated by a nucleolytic process called DNA end resection, which removes nucleotides from 5′ DSB ends. This formation of single-stranded DNA (ssDNA) by resection of DSB ends is essential for the process of Rad51-mediated strand invasion (Shibata and Jeggo, 2020; Symington and Gautier, 2011). The onset of resection blocks restorative repair by NHEJ and instead favors DSB repair by HR (Densham and Morris, 2019; Shibata and Jeggo, 2020; Symington and Gautier, 2011). Therefore, the DSB resection process is a critical step for the choice of repair pathways.

The DSB resection process is initially activated by BRCA1 (Cruz-García et al., 2014; Densham and Morris, 2019), which was originally identified based on the causative role of *brca1* mutations in familial breast cancer (Miki et al., 1994). BRCA1 binds to CtIP phosphorylated by cyclin-dependent kinase (Cruz-García et al., 2014; Densham and Morris, 2019). Phosphorylated CtIP also associates with NBS1, a component of the MRN (MRE11-RAD50-NBS1) complex, to activate MRE11 nuclease activity for the initiation of resection (Cruz-García et al., 2014; Densham and Morris, 2019; Hoa et al., 2015; Reginato and Cejka, 2020; Takeda et al., 2016). The combined action of BRCA1-CtIP and MRN-CtIP is suggested to generate a short 3′ ssDNA tail, which undergoes further DNA end resection by exonucleases such as EXO1 to create a longer stretch of ssDNA (Roy et al., 2011). Loss of either BRCA1 or CtIP results in a severe defect in HR repair, implying that the phosphorylation-dependent BRCA1-CtIP and MRN-CtIP interactions play a critical role in HR by promoting DSB resection (Cruz-García et al., 2014; Densham and Morris, 2019; Hoa et al., 2015; Huertas and Jackson, 2009).

In contrast to the HR-promoting role of the BRCA1-CtIP and MRN-CtIP interactions, the 53BP1-RIF1 complex is known to inhibit the DSB resection process to suppress HR (Bunting et al., 2010; Zimmermann and de Lange, 2014). Following DNA damage, 53BP1 accumulates on DSB sites and is phosphorylated on S/T-Q sites by ATM kinase. Phosphorylation of 53BP1 causes recruitment of RIF1, and the resulting 53BP1-RIF1 complex inhibits the accumulation of BRCA1 on DSBs and consequent resection, thereby opposing HR. RIF1 is antagonized by SCAI, a recently revealed novel 53BP1 interactor, which is recruited through phosphorylated S/T-P sites on 53BP1 (Isobe et al., 2017). SCAI binding to 53BP1 promotes the association with DSB sites of HR factors, such as BRCA1, by inhibiting RIF1 to stimulate DSB resection for HR (Isobe et al., 2017).

53BP1 is therefore subject to multiple layers of regulation involving RIF1 and SCAI to ensure an appropriate choice between NHEJ and HR repair.

Recent studies have described the Shieldin complex as an effector of 53BP1-RIF1. Shieldin consists of the SHLD1 (C20orf96), SHLD2 (FAM35A), SHLD3 (CTC-534A2.2), and REV7 proteins, which were identified as causing resistance of BRCA1-deficient cells to PARP inhibitors when mutated (Dev et al., 2018; Gupta et al., 2018; Noordermeer et al., 2018; Xu et al., 2015). Shieldin accumulates at DSBs in a 53BP1-RIF1-dependent manner (Dev et al., 2018; Findlay et al., 2018; Ghezraoui et al., 2018; Gupta et al., 2018; Mirman et al., 2018; Noordermeer et al., 2018; Setiaputra and Durocher, 2019; Tomida et al., 2018). Dysfunction of the Shieldin complex impairs repair through the NHEJ pathway (including class-switch recombination) and leads to excessive DNA end resection (Dev et al., 2018; Findlay et al., 2018; Ghezraoui et al., 2018; Gupta et al., 2018; Mirman et al., 2018; Noordermeer et al., 2018; Setiaputra and Durocher, 2019). Shieldin was shown to bind to the short stretch of ssDNA produced by CtIP and MRN, where it inhibits further resection, opposing the formation of extended ssDNA that would direct HR (Dev et al., 2018; Findlay et al., 2018; Ghezraoui et al., 2018; Noordermeer et al., 2018). Shieldin also recruits DNA polymerase α/primase (Polα) to fill in the resected ends, enabling their ligation through the NHEJ pathway (Mirman et al., 2018). The discovery of the Shieldin complex uncovered the molecular mechanism through which 53BP1-RIF1 represses extended resection and HR, which requires a relatively long stretch of ssDNA. However, the extent to which 53BP1-RIF1 steers repair pathway choice at unresected DSB ends has remained unclear.

In this study, we identify PP1 as an effector of RIF1 acting distinctly from Shieldin in the damage response. We find that PP1 suppresses the initiation of resection, apparently by inhibiting CtIP-MRN activity in the early phase of the damage response. In this role PP1 precedes the effect of Shieldin, which suppresses the extension of resection after its initiation. Our study reveals that PP1 and Shieldin work together to suppress precocious HR, supporting the retention of DNA ends in a form suitable for repair through NHEJ.

RESULTS

RIF1 suppresses CtIP IRIF independent of Shieldin function

To investigate the role of RIF1 in the damage response for DSB repair, we created RIF1 knockout (KO) HeLa cells by genome editing using a guide RNA designed 33 bp downstream of the start codon (Figure 1A). We confirmed RIF1 gene disruption by western blotting, probing with antibodies against both N and C termini of RIF1 to ensure that no truncated RIF1 is present (Figure 1B). Next, we examined how RIF1 affects DSB resection by the CtIP-MRN complex after DNA damage (Figures 1C, S1A, and S1B). In wild-type (WT) G_2 cells, irradiation-induced foci (IRIF) of CtIP were detected 1 h after X-ray irradiation and then gradually increased. In contrast, in RIF1 KO, CtIP IRIF were dramatically increased at 0.5 h, and the high level was maintained at subsequent time points (Figure 1C). The stimulation of CtIP IRIF at 0.5 h was also observed in small interfering RNA (siRNA)-induced RIF1-deficient cells (Figures S1A and S1B; Isobe et al., 2017). These results suggest that RIF1 suppresses CtIP-MRN function during the early phase of the damage response.

The Shieldin complex is an effector for RIF1 in the damage response, protecting short ssDNA tails resected by CtIP-MRN from more extended resection that would direct HR (Dev et al., 2018; Findlay et al., 2018; Ghezraoui et al., 2018; Mirman et al., 2018; Noordermeer et al., 2018; Setiaputra and Durocher, 2019). We examined the effect of removing the Shieldin component REV7 on CtIP IRIF. REV7-depleted cells showed CtIP IRIF levels similar to WT cells at all time points (Figures 1C, S1A, and S1B). Similarly, depleting another Shieldin component, SHLD2, did not significantly increase the number of CtIP IRIF compared to the control at 0.5 h (Figures S1A and S1B).

The different effect on CtIP IRIF in RIF1 KO cells and Shieldin-depleted cells 0.5 h after irradiation suggests that suppression of early-stage CtIP accumulation by RIF1 is not mediated by Shieldin. This finding also implies that Shieldin is not the sole effector for RIF1 at DSBs, and other effectors may be involved in suppressing resection by CtIP-MRN.

PP1 accumulates on DSB sites through RIF1

We used a proteomic mass spectrometry approach to search for additional RIF1 effectors, and identified all three subtypes of protein phosphatase 1 (PP1α, PP1β, and PP1γ) (Figure S2A). Consistently, PP1 was already demonstrated to be a physically associated effector of RIF1 in the regulation of DNA replication (Garzón et al., 2019; Hiraga et al., 2014, 2017; Sukackaite et al., 2017), raising the possibility that the PP1α/β/γ proteins act as RIF1 effectors also for damage repair. PP1 proteins have little intrinsic substrate specificity and are directed to specific substrates by their interacting proteins (Peti et al., 2013). Reasoning that RIF1-PP1 activity is therefore likely to be similar regardless of PP1 subtype, we analyzed PP1α as a representative of RIF1-PP1 function. To investigate whether PP1 is involved in DSB repair control by RIF1, we analyzed whether PP1α undergoes foci formation in response to irradiation. We observed that both endogenous and ectopically expressed PP1α forms IRIF that overlap with 53BP1 and γH2AX foci (Figure 2A), indicating that PP1 is recruited to DSB sites. Quantifying foci in S/G_2 phase cells revealed that PP1α accumulated on damage sites immediately after irradiation, with the number of PP1α IRIF having reached a maximum at 0.5 h. Afterward, PP1α IRIF numbers gradually reduced during the subsequent 6 h (Figure 2B). Interestingly, the dynamics of PP1α after irradiation resemble 53BP1 and RIF1 but differ from BRCA1 and CtIP, which accumulate later (Figures 1C and 2B). Given that RIF1 IRIF depend on 53BP1, we tested whether PP1α foci also depend on 53BP1, consistent with PP1 tethering through RIF1 recruited to damage sites by 53BP1 (Chapman et al., 2013; Di Virgilio et al., 2013; Escribano-Díaz et al., 2013; Isobe et al., 2017; Zimmermann et al., 2013). Indeed, depletion of either RIF1 or 53BP1 abolished PP1 IRIF formation, causing instead PP1 localization scattered over the nucleoplasm (Figures 2C and S2B). These results indicate that the recruitment of PP1 to DSB sites requires 53BP1 and RIF1. In contrast, SHLD2 or REV7 depletion did not affect the

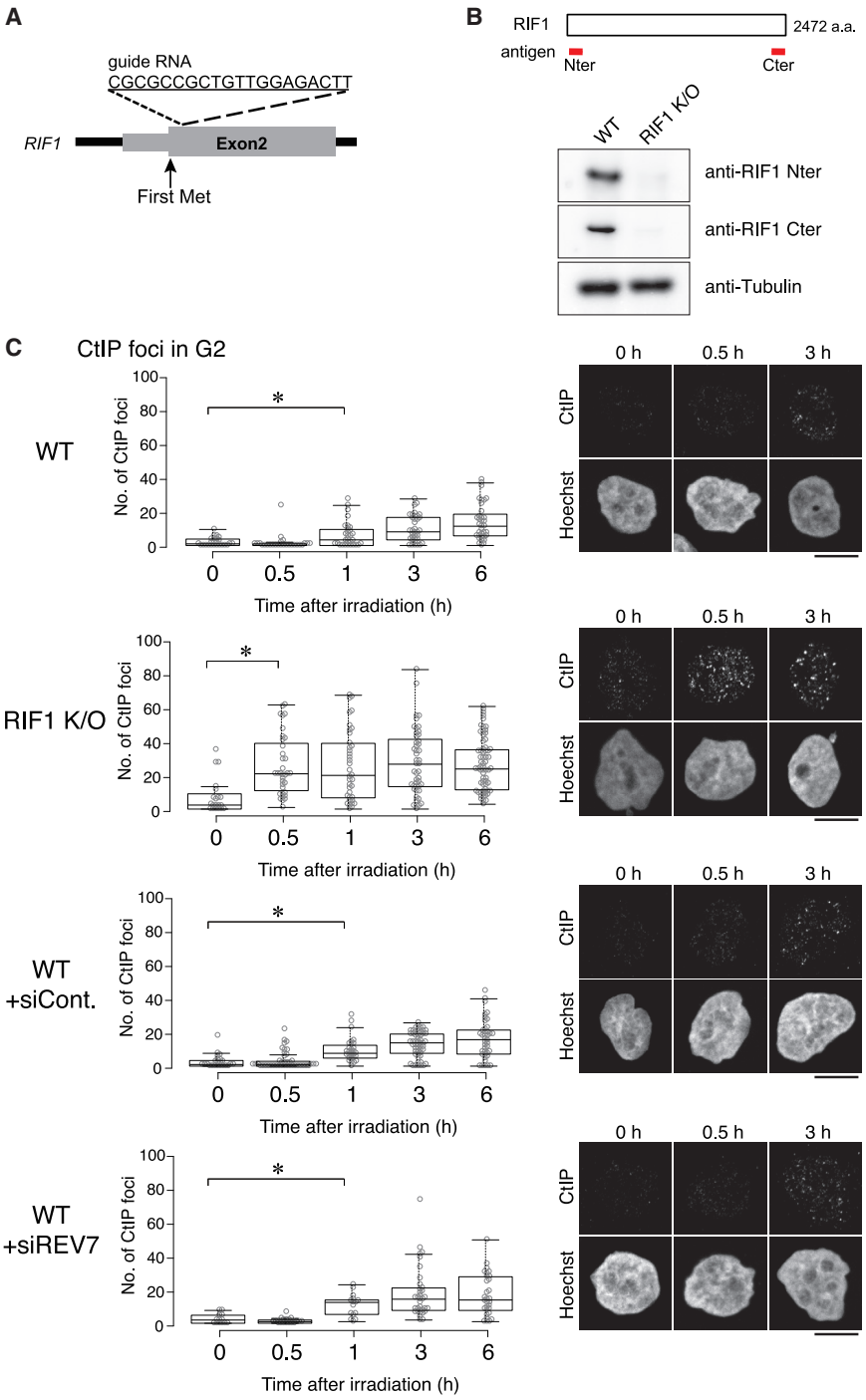

Figure 1. RIF1, but not Shieldin, suppresses CtIP IRIF

(A) Schematic diagram of RIF1 gene construct on the genome, with guide RNA sequence for disruption by CRISPR-Cas9.

(B) Western blot of whole-cell extracts prepared from wild-type (WT) cells and RIF1 knockout (KO) cells, probed with indicated antibodies. Tubulin is a loading control.

(C) CtIP IRIF in the G_2 phase. Indicated cell lines were treated with/without indicated siRNA for 48 h and then irradiated. After irradiation (3 Gy), cells were fixed at the indicated time (with addition of 5-ethynyl-2′-deoxyuridine [EdU] 10 min beforehand) and immunostained with an anti-CtIP antibody, along with Hoechst staining and EdU Click-iT visualization. Cells in the G_2 phase were assigned based on Hoechst intensity and lack of EdU signal. The numbers of CtIP foci in the G_2 phase are shown as bee swarm plots (left). p values were calculated using a Mann-Whitney U test (*$p < 0.001$). Representative images are shown for cells 0, 0.5, and 3 h post-irradiation (right). Scale bars, 10 μm.

See also Figure S1.

number of PP1 foci (Figure 2C), indicating that PP1 is recruited by RIF1 in a Shieldin-independent manner.

Previous studies have demonstrated that SCAI and BRCA1 antagonize the inhibitory effect of 53BP1 and RIF1 on HR (Chapman et al., 2013; Di Virgilio et al., 2013; Escribano-Díaz et al., 2013; Feng et al., 2013; Isobe et al., 2017; Isono et al., 2017). We sought to examine whether BRCA1 and SCAI are involved in recruitment of PP1 to DSB sites. PP1α focus formation was not affected by the depletion of either SCAI or BRCA1. Instead, we found that PP1α IRIF signal intensity and number were increased in both BRCA1- and SCAI-depleted cells compared to WT cells (Figures 2C and S2B) . This suggests that more PP1 is recruited to each damage site, potentially reflecting that the inhibition of RIF1 function by BRCA1 or SCAI is attenuated (Chapman et al., 2013; Isobe et al., 2017; Isono et al., 2017).

PP1 IRIF require direct binding of RIF1-PP1

PP1 regulates DNA metabolism and chromosome maintenance through dephosphorylation of various target substrates (Cohen, 2002). To focus on the function of PP1 in DSB repair, we analyzed cells expressing a RIF1 mutant protein that is unable to associate with PP1. To this end, we generated three versions of RIF1, mutated either at a PP1 binding motif close to the N terminus (RIF1ppN), or at two PP1 binding motifs close to the C terminus (RIF1ppC), or else mutated at all three motifs (RIF1pp) (Figure 3A; Hiraga et al., 2017). While RIF1ppN was still able to interact with PP1α, the RIF1ppC and RIF1pp mutations completely abolished PP1α interaction (Figure 3B), indicating that RIF1 associates with PP1α through its C-terminal motifs, consistent with a previous report for the mouse RIF1 protein (Sukackaite et al., 2017). We therefore used the C-terminal mutant (RIF1ppC) as a version of RIF1 lacking PP1-binding capability. Next, we established RIF1 KO cell

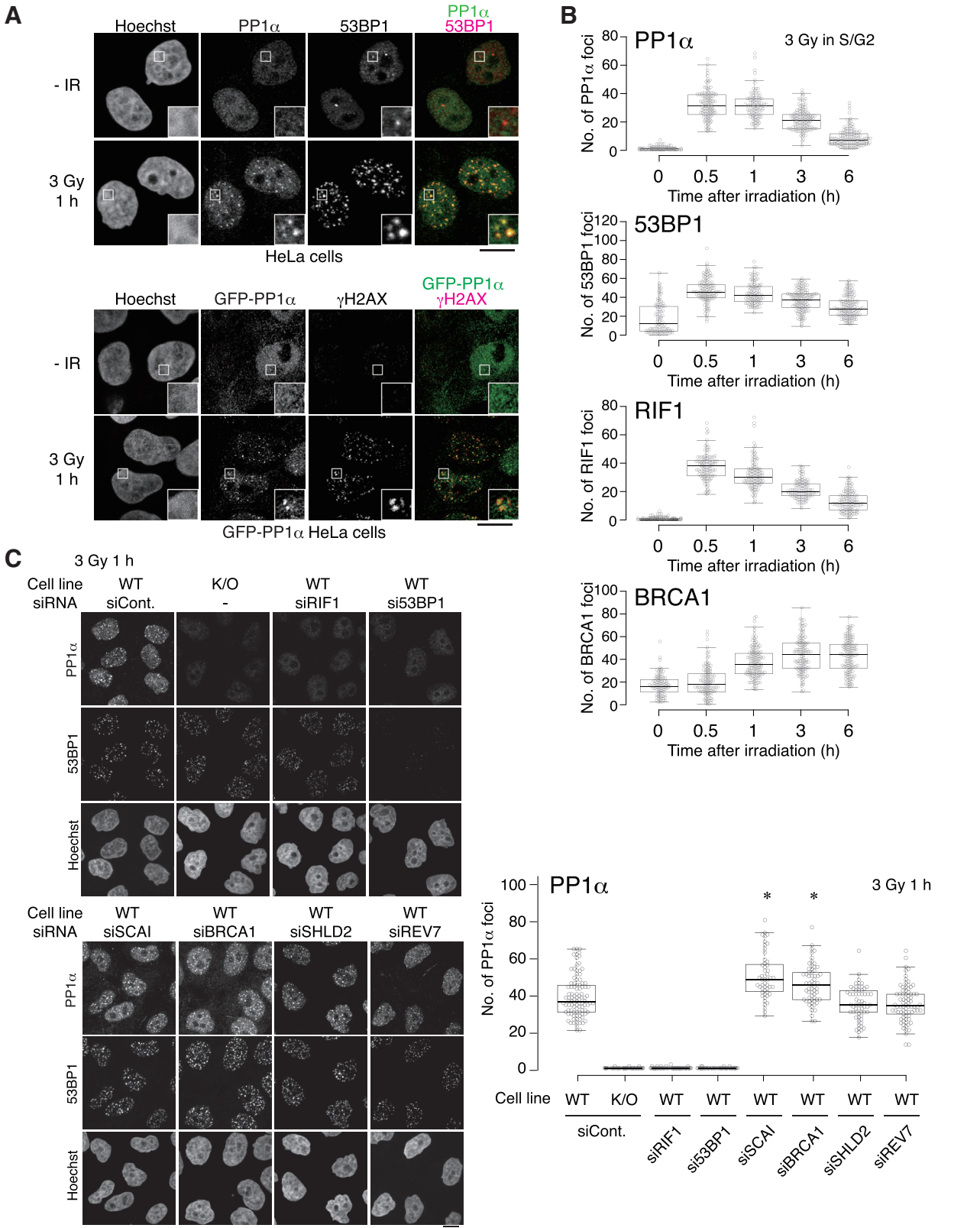

(legend on next page)

lines with FLAG-sfGFP-tagged RIF1 derivative (RIF1WT or RIF1ppC) under the control of doxycycline (Dox) promoter (designated as WT^{KI} or ppC^{KI}). 24 h after Dox induction the expression levels of RIF1WT and RIF1ppC were approximately 3-fold those of endogenous RIF1 (Figure S3). Similar to endogenous RIF1 in WT cells, RIF1WT and RIF1ppC formed IRIF that overlapped with 53BP1 (Figure 3C; Isobe et al., 2017). Furthermore, RIF1WT and RIF1ppC displayed a similar number of RIF1 IRIF, with some RIF1ppC foci appearing slightly brighter. We suspect this reflects the fact that cells expressing RIF1ppC accumulate phosphorylated 53BP1, likely due to defective DSB repair, which causes increased recruitment of RIF1 onto DSB sites. In RIF1 KO cells expressing RIF1WT (WT^{KI}), the number of PP1α IRIF was comparable to WT cells (Figure 3C), confirming that RIF1 function is properly complemented by the ectopic RIF1WT expression. In marked contrast, in RIF1 KO cells expressing RIF1ppC (ppC^{KI}), we did not detect PP1α IRIF after irradiation, despite efficient recruitment of the RIF1ppC onto DSB sites (Figure 3C). PP1 levels are similar in KO+RIF1ppC (ppC^{KI}) to WT and KO+RIF1WT cells (WT^{KI}) (Figure S3). These results therefore suggest that direct recruitment by RIF1 is responsible for PP1 IRIF formation.

RIF1-PP1 suppresses formation of CtIP IRIF in the early phase of damage response

Even though Shieldin is an effector of RIF1, the involvement of RIF1 in the early stage of the damage response differs from that of Shieldin. In particular, RIF1 suppresses CtIP IRIF formation immediately after irradiation, while Shieldin does not (Figures 1C and S1A). Considering this difference, we hypothesized that, as another effector of RIF1, PP1 might be involved in regulating CtIP IRIF formation. We therefore examined how abolishing PP1 recruitment by RIF1 affects CtIP IRIF immediately after irradiation. In the RIF1 KO cells expressing RIF1 defective for PP1 binding (ppC^{KI}), the number of CtIP IRIF was increased to a level similar to RIF1 KO cells (Figure 4A). In contrast, RIF1 KO cells expressing RIF1WT (WT^{KI}) showed a low CtIP IRIF number similar to WT cells (Figure 4A). These results suggest that PP1 is another effector of RIF1, acting separately from Shieldin, that specifically suppresses CtIP loading at DSB sites, potentially to suppress initiation of resection in the early phase of the damage response. In contrast, Shieldin knockdown (by either siREV7 or siSHLD2) hardly increased CtIP IRIF numbers 0.5 h after irradiation (Figures 1C, 4A, and S1A). Moreover, the number of CtIP IRIF in KO+RIF1ppC cells (ppC^{KI}) was hardly affected by the presence or absence of SHLD2 (Figure 4A). It therefore appears that suppression of CtIP foci by RIF1 is mediated principally by PP1 in the early phase of damage response, with the Shieldin complex playing only a minor role at this stage.

RIF1-PP1 suppresses CtIP-BRCA1 and CtIP-MRN PLA interactions

As shown above, RIF1-PP1 suppresses CtIP loading at DSB sites. Since CtIP loading at DSBs occurs through interaction of phosphorylated CtIP with BRCA1 and MRN, we examined whether RIF1-PP1 suppresses CtIP phosphorylation. We first tested the effect of RIF1-PP1 on the phosphorylation status of CtIP by an electrophoretic mobility shift assay (Wang et al., 2013). In RIF1 KO or KO+RIF1ppC cells with DNA damage, phosphorylated forms of CtIP were more abundant than in WT and KO+RIF1WT, indicating that in the absence of RIF1-PP1, CtIP phosphorylation is intensified (Figure S4A). Therefore, RIF1-PP1 might have a function in dephosphorylation of CtIP.

We next investigated the effect of RIF1-PP1 on the recruitment of CtIP-BRCA1 to DSB sites. To this end, we exposed the cells to irradiation and subsequently performed a proximity ligation assay (PLA) to test CtIP-BRCA1 interaction. Similar to CtIP IRIF, BRCA1 IRIF formation was stimulated in RIF1- or RIF1-PP1-deficient cells 0.5 h after irradiation, but it exhibited only a subtle increase in SHLD2-depleted cells (Figure 4B). Furthermore, PLA interaction between CtIP and BRCA1 was stimulated in RIF1- or RIF1-PP1-deficient cells, but not in SHLD2-depleted cells (Figures 4C and S4B). These observations indicate that RIF1-PP1 suppresses recruitment of CtIP and BRCA1 at damage sites by inhibiting the interaction of CtIP with BRCA1, probably by inhibiting CtIP phosphorylation.

In contrast to CtIP and BRCA1, the number of NBS1 foci formed in immediate response to irradiation did not differ between the cell lines examined (including RIF1- or RIF1-PP1-deficient cells), indicating that loading of MRN at damage sites is independent of RIF1 (Figure 4B; Falck et al., 2012). Nor were NBS1 foci affected by siRNA against SHLD2. However, PLA interaction between CtIP and NBS1 was increased in RIF1 KO and in KO+RIF1ppC cells (Figures 4C and S4B). These results suggest that phosphorylated CtIP associates with MRN through NBS1 on damage sites, and RIF1-PP1 might suppress the CtIP-MRN association through dephosphorylation of CtIP, in turn preventing the initiation of resection.

RIF1-PP1 contributes to suppression of MRN exonuclease-dependent resection in the early phase of the damage response

In PLA experiments we discovered enhanced interactions of CtIP-BRCA1 and CtIP-NBS1 in RIF1-PP1-deficient cells (Figure 4C). These findings raise the possibility of elevated initiation

Figure 2. PP1 IRIF depends on RIF1

(A) PP1α IRIF. HeLa cells (upper) or HeLa cells stably expressing GFP-PP1α (lower) were irradiated (3 Gy) and then 1 h later fixed for immunostaining with anti-PP1α, anti-53BP1, and anti-γH2AX antibodies. GFP-PP1α was detected as GFP signal. Scale bars, 10 μm.

(B) Time course analysis of IRIF for PP1α, 53BP1, RIF1, and BRCA1 in S/G_2 cells. Cells were irradiated (3 Gy) and incubated for the indicated periods prior to fixation for immunofluorescence. Cells were immunostained with antibodies against indicated proteins and cyclin A, along with Hoechst staining. Cells in the S/G_2 phase were assigned based on cyclin A intensity. Numbers of foci are shown as a bee swarm plot.

(C) Dependency of PP1 IRIF on RIF1 and 53BP1. WT or RIF1 KO cells were treated with indicated siRNA for 48 h and irradiated (3 Gy) and then 1 h later fixed for immunostaining with anti-PP1α and anti-53BP1 antibodies. The numbers of PP1α foci are shown as bee swarm plots ($p < 0.001$ for WT siCont). Scale bar, 10 μm. See also Figure S2.

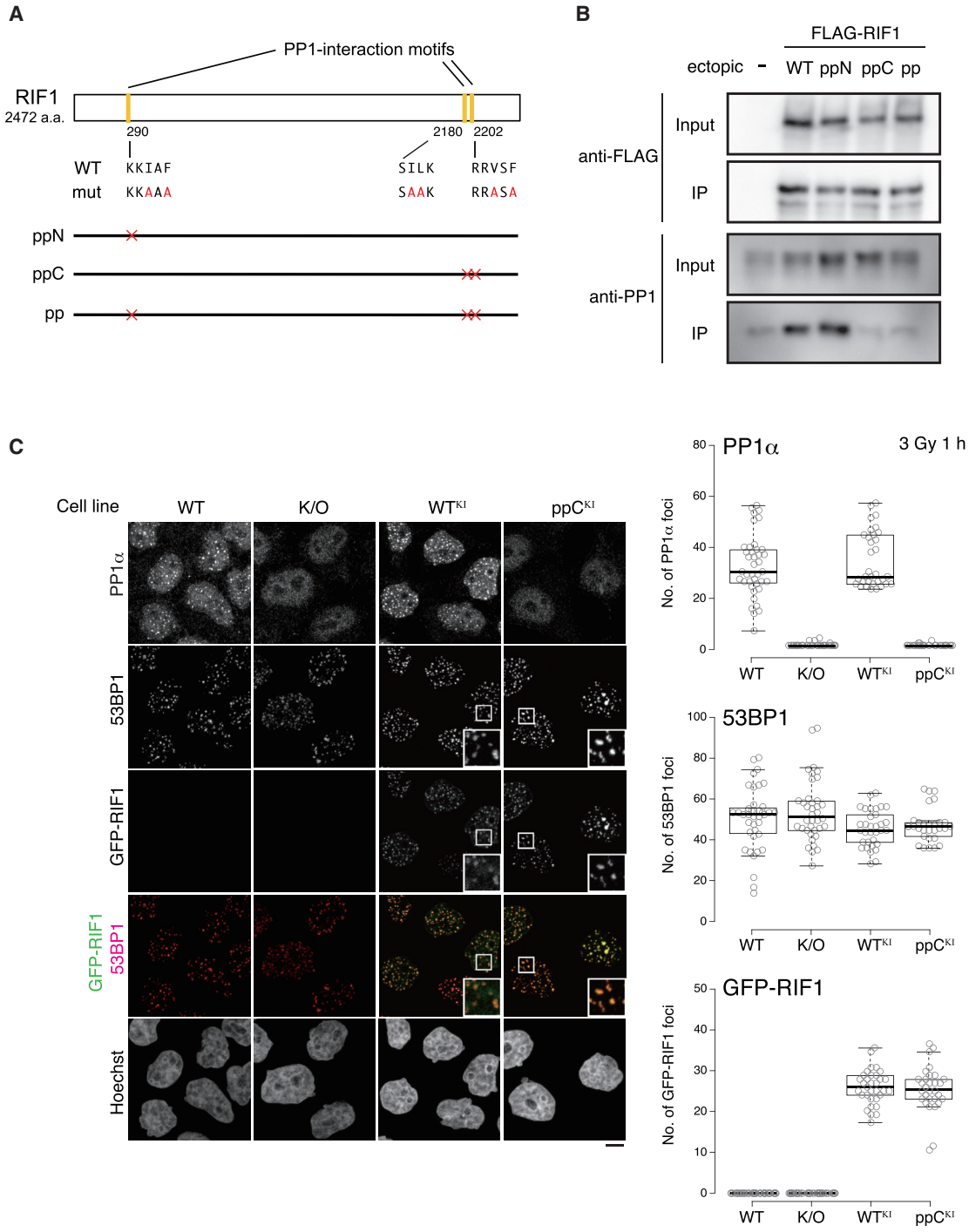

Figure 3. PP1 IRIF depends on the direct binding to RIF1

(A) Schematic structure of RIF1 indicating its three PP1 binding motifs and the mutants created.

(B) Testing PP1 binding for the mutants created. T-REx 293 cells were transfected with expression plasmids for the indicated constructs. FLAG-RIF1 immunoprecipitates were analyzed by western blotting by the indicated antibodies.

(C) Cell lines with endogenous RIF1 replaced by the mutant deficient in PP1 binding. Cells were irradiated (3 Gy) 24 h after doxycycline (Dox) induction. Then, 1 h later, the cells were fixed for immunostaining with anti-PP1α and anti-53BP1 antibodies. KO+RIF1WT (WT^{KI}), RIF1 KO cell with Dox-inducible FLAG-sfGFP-tagged WT RIF1; KO+RIF1ppC (ppC^{KI}), RIF1 KO cell with Dox-inducible FLAG-sfGFP-tagged mutant deficient in PP1 binding. Dox-induced FLAG-sfGFP-tagged RIF1 derivatives were detected as GFP signal. The numbers of GFP-tagged RIF1 derivatives, PP1α, and 53BP1 foci are shown as bee swarm plots. Scale bar, 10 μm. See also Figure S3.

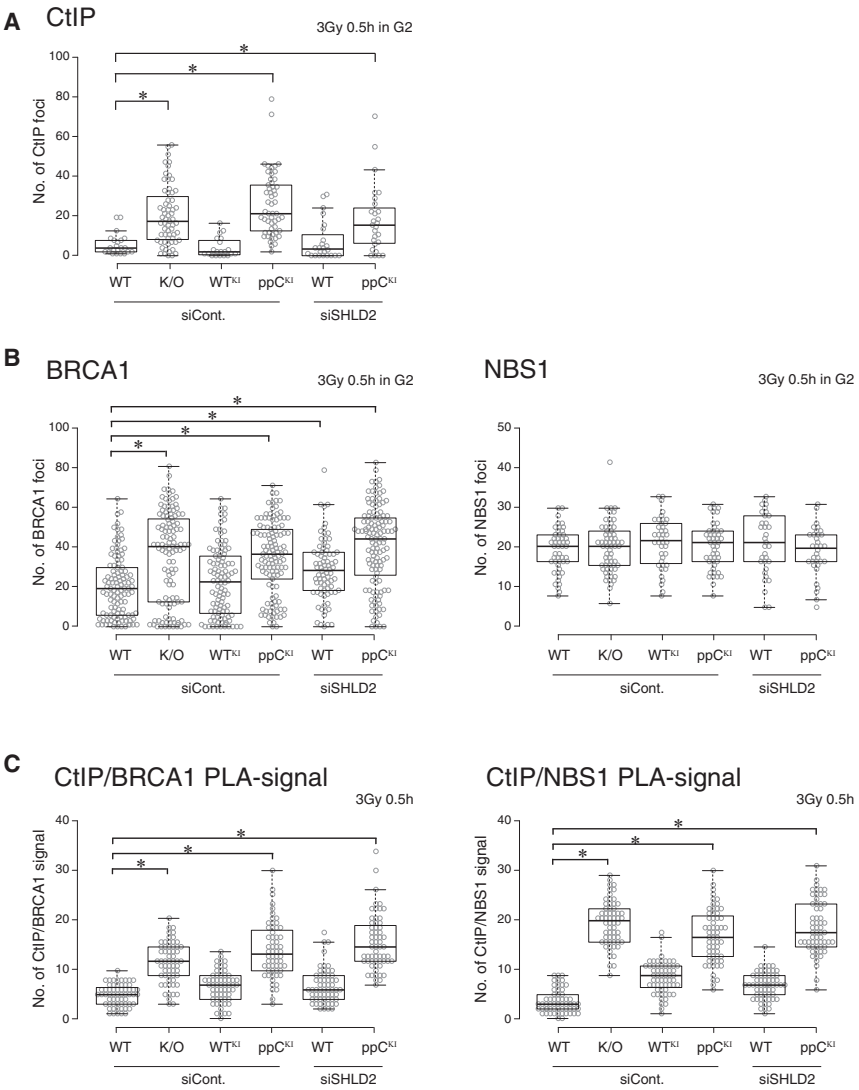

Figure 4. RIF1-PP1 interaction suppresses CtIP and BRCA1 IRIF and limits CtIP-BRCA1 and CtIP-NBS interactions as assessed by PLA

(A) RIF1 function in CtIP IRIF in G_2 cells. 48 h after transfection by siRNA and 24 h after Dox addition, the indicated cell lines were irradiated (3 Gy) 0.5 h before fixation (with EdU addition 10 min before fixation). Cells were immunostained with anti-CtIP antibody, along with Hoechst staining and EdU Click-iT visualization. Cells in the G_2 phase were assigned as in Figure 1C. WT^{KI} (KO+RIF1WT cell) and ppC^{KI} (KO+RIF1ppC cell) as in Figure 3C. Numbers of CtIP foci in G_2 phase cells are shown as bee swarm plots. p values were calculated using a Mann-Whitney U test (*$p < 0.001$).

(B) Effect of RIF1 on BRCA1 and NBS1 IRIF. 48 h after transfection by siRNA and 24 h after Dox addition, indicated cell lines were irradiated (3 Gy) 0.5 h before fixation. Cells were immunostained with anti-BRCA1 or anti-NBS1 antibodies along with cyclin A immunostaining and Hoechst staining. The G_2 cells were assigned based on cyclin A intensity. WT^{KI} and ppC^{KI} are as in Figure 3C. Numbers of BRCA1 (left) or NBS1 (right) foci in the G_2 phase are shown as bee swarm plots. p values were calculated using a Mann-Whitney U test (*$p < 0.001$).

(C) Effect of RIF1 on BRCA1-CtIP and NBS1-CtIP interaction tested by PLA. 48 h after transfection by siRNA and 24 h after Dox addition, indicated cell lines were irradiated (3 Gy) 0.5 h before fixation. Cells were immunostained with anti-CtIP antibody and anti-BRCA1 or anti-NBS1 antibodies, and then *in situ* ligation and amplification reactions were performed. DNA was stained with DAPI. WT^{KI} and ppC^{KI} are as in Figure 3C. Numbers of PLA signal in nucleolus are shown as bee swarm plots. p values were calculated using a Mann-Whitney U test (*$p < 0.001$).

See also Figure S4.

of resection with an increase in short ssDNA exposure due to CtIP-MRN activity. To examine this possibility, we visualized ssDNA-binding protein RPA as a proxy for ssDNA caused by end resection. In RIF1 KO cells and in cells expressing RIF1 incapable of PP1 binding, the number of RPA foci was increased at 0.5 h after irradiation, compared to control cells (compare columns 1, 3, and 7, Figure 5A). An increased number of RPA foci was also observed in SHLD2-depleted cells (column 9). To investigate how an effect of RIF1-PP1 on MRE11 nuclease activity may contribute to ssDNA and RPA foci, we treated cells with the MRE11 exonuclease inhibitor Mirin before irradiation. The increase in RPA foci in KO+RIF1ppC cells was completely abolished by mirin treatment, indicating that the ssDNA caused by loss of RIF1-PP1 is generated by MRE11 exonuclease activity (column 8, Figure 5A). In contrast, RPA foci in SHLD2-depleted cells were hardly affected by mirin (column 10), suggesting that the elevated RPA foci in Shieldin-depleted cells reflect ssDNA resection by an exonuclease other than MRN, possibly Exo1.

We conclude that PP1 is an effector of RIF1 acting quite distinct from Shieldin, and it is particularly involved in suppressing ssDNA exposure by inhibiting the initiation of resection by CtIP-MRN in the early phase of the damage response. In the case of RIF1 KO cells, the increase in RPA foci 0.5 h after irradiation was noticeably but not completely prevented by mirin treatment (column 4, Figure 5A). We interpret the mirin-resistant increase in RPA in RIF1 KO cells as indicative of ssDNA occurring due to failed Shieldin recruitment. The substantial effect of mirin 0.5 h after irradiation indicates the important contribution of PP1 for RIF1 function immediately after irradiation, when its effect dominates over that of Shieldin.

PP1 cooperates with Shieldin to suppress HR repair in the early phase of the damage response

To further investigate the functional relationship between PP1 and Shieldin as effectors of RIF1, we analyzed IRIF of RAD51, a marker for HR (Figure 5B). At 0.5 h post-irradiation, we found

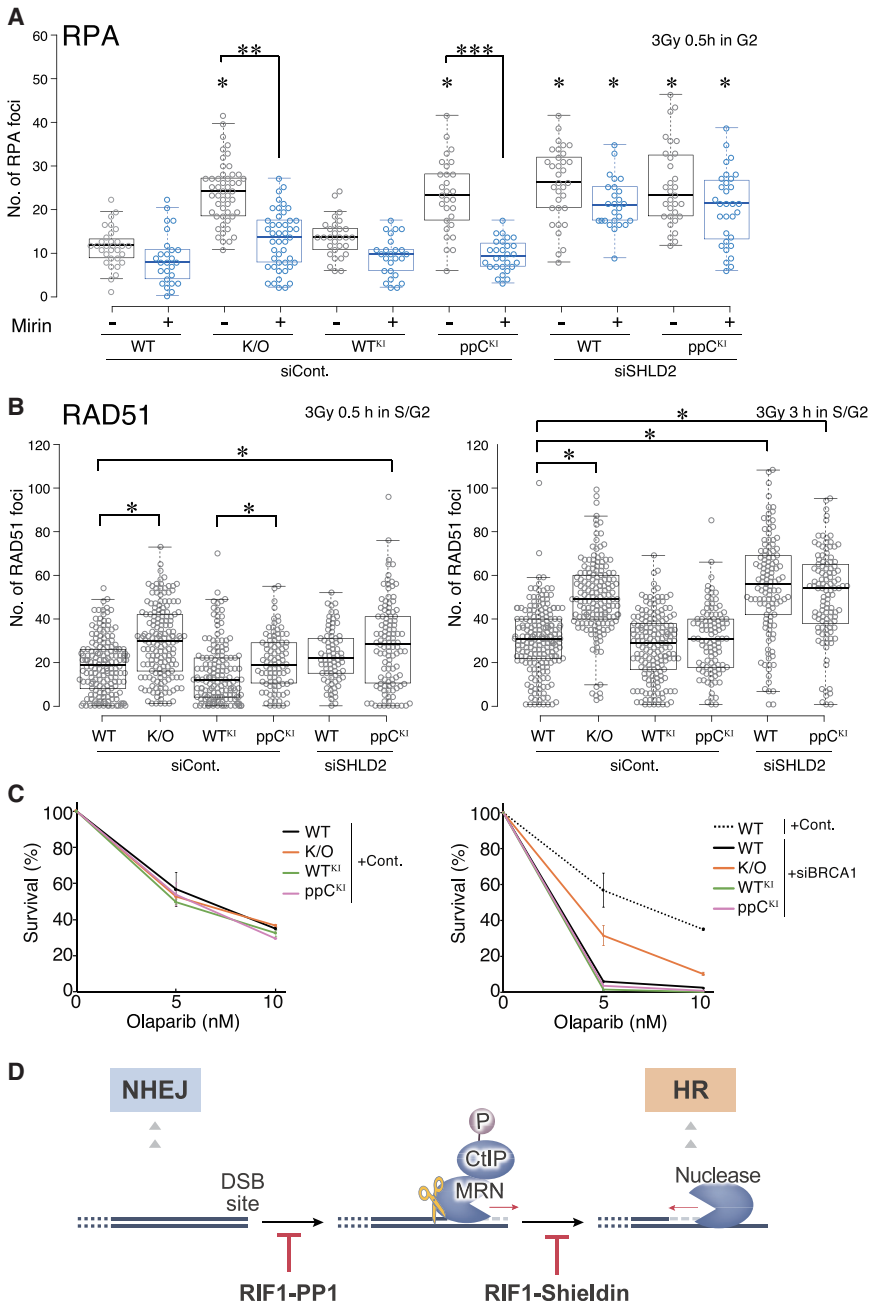

Figure 5. Suppression of precocious HR by PP1 in cooperation with Shieldin

(A) RIF1 effect on RPA IRIF in G_2 cells. 48 h after transfection by siRNA and 24 h after Dox addition, indicated cell lines were irradiated (3 Gy) 0.5 h before fixation (with addition of EdU 10 min beforehand) in the absence or the presence of the MRE11 exonuclease inhibitor mirin. Cells were immunostained with anti-RPA2, along with Hoechst staining and EdU Click-iT visualization. Cells in the G_2 phase were assigned as in Figure 1C. WT^{KI} and ppC^{KI} are as in Figure 3C. The numbers of RPA2 IRIF in the G_2 phase cells are shown as bee swarm plots. p values were calculated using a Mann-Whitney U test (*$p < 0.001$ for WT + siCont; **,***$p < 0.001$ for the respective no-mirin conditions).

(B) RIF1 function in RAD51 IRIF in S/G_2 cells. 48 h after transfection by siRNA and 24 h after Dox addition, the indicated cell lines were irradiated (3 Gy) 0.5 or 3 h before fixation. Cells were immunostained with anti-RAD51 and anti-cyclin A antibodies with Hoechst staining. Cells in the S/G_2 phase were assigned based on cyclin A intensity. WT^{KI} and ppC^{KI} are as in Figure 3C. The numbers of RAD51 IRIF in the S/G_2 phase cells are shown as bee swarm plots. p values were calculated using a Mann-Whitney U test (*$p < 0.001$).

(C) Olaparib sensitivity in BRCA1-deficient cells. The cells were treated with olaparib for 72 h after transfection with siRNA against control (left) or BRCA1 (right), plating a fixed number of cells, and Dox addition. During the period for olaparib treatment, RIF1WT and RIF1ppC were constantly supplied by Dox induction even in the presence or absence of BRCA1 or olaparib (Figure S5A). Indicated cell lines treated with either control or BRCA1 siRNA was examined using a colony formation assay (Figure S5B). WT^{KI} and ppC^{KI} are as in Figure 3C. Numbers of colonies were standardized relative to those not treated with PARP inhibitor (mean ± SD; n = 2 experiments).

(D) Model for function of RIF1 in the damage response with two effectors, PP1 and Shieldin. RIF1 negatively regulates HR and directs NHEJ through two distinct pathways: through PP1 recruitment inhibiting initiation of resection, and through Shieldin recruitment inhibiting further, extended resection. See Discussion for details. See also Figure S5.

a significant increase in RAD51 IRIF in RIF1 KO cells when compared with WT (Figure 5B, left), indicating that RIF1 is required to suppress HR in the early stage of the damage response. A significant increase in RAD51 IRIF was also observed in cells expressing RIF1 incapable of PP1 binding (KO+RIF1ppC) when compared to KO+RIF1WT cells, but the extent was less than in RIF1-deficient cells. No increase in RAD51 IRIF was, however, observed in Shieldin-depleted cells, compared with WT (Figure 5B, left). These data suggest that the RIF1-PP1 pathway is dominant in suppressing HR in the early stage of the damage response, with the effect of the RIF1-Shieldin pathway being minimal when RIF1-PP1 is functional. However, combined loss of RIF1-PP1 interaction and Shieldin depletion caused a further increase in RAD51 IRIF number, with an effect similar to RIF1 KO (Figure 5B, left). This result suggests that PP1 and Shieldin function independently, and Shieldin has little function in suppressing HR at the early stage. However, when resection is initiated by CtIP-MRN in the absence of RIF1-PP1 activity, Shieldin is required to suppress further extension of ssDNA for HR (Dev et al., 2018; Findlay et al., 2018; Ghezraoui et al., 2018; Gupta et al., 2018; Mirman et al., 2018; Noordermeer et al., 2018; Tomida et al., 2018). RIF1 deletion also increased the

number of RAD51 IRIF even at 3 h post-irradiation (Figure 5B, right). At this later stage, we found that SHLD2 depletion increased the number of RAD51 IRIF independent of PP1 function, indicating that the relative contribution of Shieldin to HR inhibition increases at later phase of damage response. This finding is consistent with reports that a functional deficiency in Shieldin alone promotes HR (Findlay et al., 2018; Tomida et al., 2018). In summary, we find that PP1 delays the onset of HR principally in the early response phase, whereas the contribution made by Shieldin to HR suppression increases as the response develops.

PP1 did not show suppression of PARP inhibitor sensitivity in the BRCA1-depleted background

We showed that RIF1-PP1 function in suppression of HR is limited to the early response phase, followed by a larger contribution of RIF1-Shieldin at a later stage. Therefore, we hypothesized that even if PP1 recruitment by RIF1 fails, RIF1-Shieldin function is nonetheless ultimately sufficient to protect DNA ends and direct cells to use NHEJ. To test this possibility, we examined the sensitivity of BRCA1-depleted RIF1 KO cells to the PARP inhibitor olaparib by clonogenic cell survival assay. This test is based on the supposition that olaparib generates one-ended DSBs in S phase cells, which must be repaired predominantly by HR for survival (Lord and Ashworth, 2013). It was previously shown that either RIF1 or Shieldin depletion suppresses the sensitivity of BRCA1-deficient cells to olaparib, presumably because enhanced resection in the absence of Shieldin can promote HR even when BRCA1 is lacking (Escribano-Díaz et al., 2013; Findlay et al., 2018; Ghezraoui et al., 2018; Gupta et al., 2018; Mirman et al., 2018; Noordermeer et al., 2018; Xu et al., 2015). If deficiency of RIF1-PP1 function can be compensated by RIF1-Shieldin, then failure of RIF1 to recruit PP1 will not suppress sensitivity to olaparib in the BRCA1-depleted context.

For the clonogenic cell survival assay, a fixed number of cells was plated with Dox induction, then 24 h later the cells were treated with olaparib for 72 h (Figures 5C, S5A, and S5B). In the presence of BRCA1, RIF1 KO cells, RIF1 KO cells expressing RIF1WT, and RIF1 KO cells expressing RIF1 lacking PP1 binding did not show olaparib sensitivity, compared with WT cells. As previously demonstrated, in the BRCA1-depleted background, RIF1 KO partially suppressed the sensitivity to PARP inhibitor (Figure 5C; Dev et al., 2018; Escribano-Díaz et al., 2013; Noordermeer et al., 2018; Xu et al., 2015). Notably, however, the BRCA1-depleted RIF1 KO cells expressing RIF1 deficient for PP1 binding showed no suppression of PARP inhibitor sensitivity, but rather they showed sensitivity similar to BRCA1-depleted WT cells (Figure 5C). These results indicate that the RIF1-Shieldin pathway can compensate for defects in the RIF1-PP1 pathway to maintain sensitivity to olaparib-induced DNA damage. To confirm this idea, we performed reporter assays directly monitoring repair through NHEJ or HR at a site-specific DSB (Figure S5C). Consistent with the results from a clonogenic cell survival assay, RIF1-depleted cells expressing mCherry-tagged RIF1ppC showed similar HR and NHEJ frequencies to control cells (compare columns 1, 5, and 6 in graphs). In marked contrast, Shieldin depletion (column 7) significantly enhanced HR and suppressed NHEJ frequencies as observed in RIF1 depletion (column 4). Furthermore, γH2AX kinetics showed damage persistence, with an increased number of γH2AX IRIF observed at 8 h in RIF1- or SHLD2-deficient situations (Shibata et al., 2011). RIF1-PP1 deficiency alone, however, did not result in damage persistence (Figure S5D). These observations support our model where RIF1-PP1 acts to regulate resection primarily early in the damage response, acting in a different stage of the pathway from the RIF1-Shieldin axis (Figure 5D). Moreover, these results support the idea that despite early over-recruitment of CtIP that induces precocious initiation of resection when RIF1-PP1 is absent, Shieldin can nonetheless compensate at a later stage for PP1 deficiency to ultimately support the use of NHEJ.

DISCUSSION

53BP1-RIF1 is a critical interaction for the correct choice of NHEJ-mediated repair in the damage response (Zimmermann and de Lange, 2014). In this study, we have shown that PP1 acts alongside Shieldin as an effector of RIF1 in directing DSB repair (Figure 5D).

Previous studies have shown that Ku70/80 binds rapidly to DSBs, allowing NHEJ to make the first repair attempt in the absence of resection (Britton et al., 2013; Frank-Vaillant and Marcand, 2002; Kim et al., 2005; Shibata et al., 2011; Shibata and Jeggo, 2020). Our results suggest that RIF1-PP1 plays a role in this situation. This study shows that PP1 binds to RIF1 at damage sites and inhibits CtIP IRIF. Consistently, RIF1-PP1 suppressed early RPA focus formation. RPA focus formation in the absence of RIF1-PP1 was mirin-sensitive; thus, RIF1-PP1 inhibits initiation of CtIP-MRN-mediated resection that provides ssDNA for Shieldin engagement. This effect of RIF1-PP1 potentially promotes NHEJ for immediate damage repair (Figure 5D). If NHEJ does not ensue (Reginato and Cejka, 2020; Shibata et al., 2011; Shibata and Jeggo, 2020), phosphorylated CtIP stimulates MRN nuclease to produce short resected ssDNA ends (Hoa et al., 2015; Huertas and Jackson, 2009; Reginato and Cejka, 2020; Sartori et al., 2007; Symington and Gautier, 2011; Takeda et al., 2016). Shieldin binds to the ssDNA at this stage to prevent extended resection that would direct repair toward HR (Dev et al., 2018; Findlay et al., 2018; Ghezraoui et al., 2018; Mirman et al., 2018; Noordermeer et al., 2018; Setiaputra and Durocher, 2019; Tomida et al., 2018): after the refilling of ssDNA by Polα, the Shieldin-bound ssDNA ends can be repaired by NHEJ (Mirman et al., 2018; Setiaputra and Durocher, 2019). RIF1-PP1 might also protect such re-filled ends from renewed resection to keep them in a state suitable for joining. If NHEJ does not ensue, Shieldin protection would be lifted, clearing the way for further end resection by exonuclease activities such as MRE11 and EXO1 to produce a length of ssDNA sufficient for HR (Dev et al., 2018; Findlay et al., 2018; Ghezraoui et al., 2018; Mirman et al., 2018; Noordermeer et al., 2018; Setiaputra and Durocher, 2019; Tomida et al., 2018). Therefore, we propose that RIF1 negatively regulates HR and directs NHEJ by distinct two pathways: through PP1 to inhibit short-range resection by CtIP-MRN, and then by Shieldin recruitment to inhibit further extended resection (Figure 5D).

RIF1-PP1 functions with Shieldin to prevent HR as monitored by visualizing RAD51 IRIF, with this role significant mainly in the early phase of damage response. We assume that, during this period, DSBs with appropriate clean ends will be repaired by NHEJ without initiation of resection (Figure 5D). The fact that the function of PP1 acts primarily early in the response and can be superseded by the alternative effector Shieldin may explain why in several reports the deficiency of RIF1 and Shieldin appears to be equivalent in terms of downstream phenotypes, such as the suppression of PARP inhibitor sensitivity in BRCA1-deficient cells, and the loss of immunoglobulin class-switch recombination (Chapman et al., 2013; Dev et al., 2018; Di Virgilio et al., 2013; Escribano-Díaz et al., 2013; Feng et al., 2013; Findlay et al., 2018; Ghezraoui et al., 2018; Mirman et al., 2018; Noordermeer et al., 2018; Setiaputra and Durocher, 2019; Tomida et al., 2018; Zimmermann et al., 2013). Furthermore, NHEJ is defective to a similar extent in RIF1- and Shieldin-deficient cells, implying that Shieldin is indeed the major effector of RIF1 for directing NHEJ (Dev et al., 2018; Ghezraoui et al., 2018; Mirman et al., 2018; Noordermeer et al., 2018; Setiaputra and Durocher, 2019). Most likely, if RIF1-PP1 deficiency causes inappropriate short-range resection at damage that should have been repaired by NHEJ prior to any resection, then the situation can still subsequently be rescued by Shieldin-regulated NHEJ, thus obscuring the effect of RIF1-PP1 deficiency on NHEJ repair rates. Indeed, unlike RIF1-Shieldin deficiency, RIF1-PP1 deficiency did not show any suppression of PARP inhibitor sensitivity in BRCA1-deficient cells, consistent with no consequences for NHEJ or HR efficiency, or for γH2AX kinetics. Through the RIF1-Shieldin pathway it is proposed that DSB ends resected by CtIP-MRN are re-filled by Polα, and then repaired by NHEJ. Shieldin has been described as promoting this pathway of NHEJ. In these considerations, RIF1 has two different functions, suppression of short-range resection (mediated by PP1) and suppression of longer-range resection (mediated by Shieldin), but with both pathways operating to protect against HR and stimulate NHEJ (Figure 5D). Intriguingly, it has been proposed that Shieldin is not always required to mediate effects 53BP1-RIF1 in repair control. During the development of immune cells distinct NHEJ pathways operate, one Shieldin-dependent and the other Shieldin-independent (Ghezraoui et al., 2018), raising the possibility that RIF1-PP1 may be required for correct pathway choice under some circumstances.

An important question is how PP1 regulates DSB repair. PP1 is a conserved Ser/Thr protein phosphatase with indiscriminate specificity *in vitro* (Cohen, 2002). RIF1 is a one of many PP1 adaptor proteins that target PP1 to physiologically relevant substrates or cellular locations (Trinkle-Mulcahy et al., 2006). In DNA replication, it has been reported that RIF1-PP1 is involved in multiple steps, including suppression of replication initiation at origins and preventing the degradation of nascent DNA at stalled forks (Garzón et al., 2019; Hiraga et al., 2017). In replication, RIF1-PP1 therefore appears to have several direct or indirect target substrates (Garzón et al., 2019; Hiraga et al., 2017). Our study indicates that RIF1-PP1 inhibits resection by MRN. MRN-mediated resection is stimulated by phosphorylated CtIP, suggesting that the relevant substrate of RIF1-PP1 might be one or more of these proteins. It has been reported that the phosphorylation of CtIP is required for a complex formation with BRCA1 and stimulation of MRN endonuclease activity to facilitate the initiation of resection (Anand et al., 2019; Cruz-García et al., 2014; Reginato and Cejka, 2020). One possible mechanism is that PP1 may dephosphorylate CtIP to prevent it from binding to BRCA1 and MRN, thereby inhibiting resection. Consistently, this study showed possible involvement of RIF1-PP1 in dephosphorylation of CtIP and suppression of CtIP-BRCA1 and CtIP-NBS interactions as assessed by PLA. Additional mechanisms may also operate, and another candidate substrate of RIF1-PP1 is 53BP1 itself. Several S/T-Q phosphorylation sites for ATM kinase close to the N terminus of 53BP1 are required for RIF1 binding (Zimmermann and de Lange, 2014). These were suggested to be dephosphorylated by PP4 to lift the block to resection by releasing RIF1 from 53BP1 (Isono et al., 2017). In contrast, several S/T-P phosphorylation sites close to the N terminus of 53BP1 are potentially phosphorylated by cyclin-dependent kinase or mitogen-activated protein kinase (MAPK) and are responsible for SCAI binding (Isobe et al., 2017). Once SCAI binds, it inhibits RIF1 and stimulates BRCA1 IRIF (Isobe et al., 2017), so RIF1-PP1 could potentially inhibit BRCA1-CtIP by preventing SCAI binding to 53BP1, possibly through dephosphorylating the S/T-P phosphorylation sites on the 53BP1. Furthermore, DNA-PKcs (DNA-dependent protein kinase, catalytic subunit), which is directly involved in NHEJ, might be a candidate substrate of RIF1-PP1. It has been shown that PP1 dephosphorylates autophosphorylated residues at the N and C termini of DNA-PKcs to cause activation (Zhu et al., 2017). Considering the RIF1 contribution to NHEJ, one possibility is that RIF1 directs the PP1, which dephosphorylates DNA-PKcs to predominantly induce NHEJ (Zhu et al., 2017). Of course, multiple layers of dephosphorylation-mediated control could affect DNA-PKcs, BRCA1, CtIP, the MRN complex, 53BP1, RIF1, PP1, and SCAI to ensure that NHEJ and HR are accurately conducted.

In summary, our results demonstrate that PP1 functions as a RIF1 effector that counteracts initiation of resection at an early stage of repair, promoting NHEJ-mediated repair prior to Shieldin function. Having established this role for RIF1-PP1, further elucidation of PP1 and Shieldin functions as effectors for RIF1 in the damage response will substantially enhance our understanding of robust and flexible repair pathway choice.

STAR★METHODS

Detailed methods are provided in the online version of this paper and include the following:

- KEY RESOURCES TABLE
- RESOURCE AVAILABILITY
  - Lead contact
  - Materials availability
  - Data and code availability
- EXPERIMENTAL MODEL AND SUBJECT DETAILS
- METHOD DETAILS
  - Drug treatment
  - RNA interference
  - Antibodies

- Plasmid construction
- Plasmid transfection and establishment of cell lines
- Immunofluorescence and microscopy
- Proximity ligation assay (PLA)
- Western blotting and immunoprecipitation
- Mass spectrometry analysis
- Quantitative real-time PCR
- Colony formation assay
- DSB reporter assay

● QUANTIFICATION AND STATISTICAL ANALYSIS

SUPPLEMENTAL INFORMATION

Supplemental information can be found online at https://doi.org/10.1016/j.celrep.2021.109383.

ACKNOWLEDGMENTS

We thank K. Murakami, H. Kimura, H. Kurumizaka, and J.M. Stark for materials. This work was supported by JSPS KAKENHI grant nos. JP19H03156, JP18H04713, JP18H05532, and JP25116004 (to C.O.), JP17H06426 (to K.N.), JP18H04900 and JP19H04267 (to H.S.), the Mitsubishi Foundation (to H.S.), and by Cancer Research UK awards C1445/A19059 and DRCPGM/100013 (to S.H. and A.D.D. lab).

AUTHOR CONTRIBUTIONS

C.O. and S.-Y.I. conceived and designed the experiments. S.-Y.I. performed most of the experiments and analyses. S.-H. and A.D.D. were involved in experiments for RIF1. H.S. was involved in experiments for damage response. K.N. performed the bioinformatics analysis. C.O. and S.-Y.I. wrote the manuscript, and A.D.D., S.H., and H.S. reviewed and edited the manuscript.

DECLARATION OF INTERESTS

The authors declare no competing interests.

Received: November 10, 2020
Revised: April 14, 2021
Accepted: June 21, 2021
Published: July 13, 2021

REFERENCES

Anand, R., Jasrotia, A., Bundschuh, D., Howard, S.M., Ranjha, L., Stucki, M., and Cejka, P. (2019). NBS1 promotes the endonuclease activity of the MRE11-RAD50 complex by sensing CtIP phosphorylation. EMBO J. *38*, e101005.

Britton, S., Coates, J., and Jackson, S.P. (2013). A new method for high-resolution imaging of Ku foci to decipher mechanisms of DNA double-strand break repair. J. Cell Biol. *202*, 579–595.

Bunting, S.F., Callén, E., Wong, N., Chen, H.T., Polato, F., Gunn, A., Bothmer, A., Feldhahn, N., Fernandez-Capetillo, O., Cao, L., et al. (2010). 53BP1 inhibits homologous recombination in *Brca1*-deficient cells by blocking resection of DNA breaks. Cell *141*, 243–254.

Chapman, J.R., Barral, P., Vannier, J.B., Borel, V., Steger, M., Tomas-Loba, A., Sartori, A.A., Adams, I.R., Batista, F.D., and Boulton, S.J. (2013). RIF1 is essential for 53BP1-dependent nonhomologous end joining and suppression of DNA double-strand break resection. Mol. Cell *49*, 858–871.

Cohen, P.T. (2002). Protein phosphatase 1—Targeted in many directions. J. Cell Sci. *115*, 241–256.

Cruz-García, A., López-Saavedra, A., and Huertas, P. (2014). BRCA1 accelerates CtIP-mediated DNA-end resection. Cell Rep. *9*, 451–459.

Densham, R.M., and Morris, J.R. (2019). Moving mountains—The BRCA1 promotion of DNA resection. Front. Mol. Biosci. *6*, 79.

Dev, H., Chiang, T.W., Lescale, C., de Krijger, I., Martin, A.G., Pilger, D., Coates, J., Sczaniecka-Clift, M., Wei, W., Ostermaier, M., et al. (2018). Shieldin complex promotes DNA end-joining and counters homologous recombination in BRCA1-null cells. Nat. Cell Biol. *20*, 954–965.

Di Virgilio, M., Callen, E., Yamane, A., Zhang, W., Jankovic, M., Gitlin, A.D., Feldhahn, N., Resch, W., Oliveira, T.Y., Chait, B.T., et al. (2013). Rif1 prevents resection of DNA breaks and promotes immunoglobulin class switching. Science *339*, 711–715.

Difilippantonio, S., Gapud, E., Wong, N., Huang, C.Y., Mahowald, G., Chen, H.T., Kruhlak, M.J., Callen, E., Livak, F., Nussenzweig, M.C., et al. (2008). 53BP1 facilitates long-range DNA end-joining during V(D)J recombination. Nature *456*, 529–533.

Escribano-Díaz, C., Orthwein, A., Fradet-Turcotte, A., Xing, M., Young, J.T., Tkáč, J., Cook, M.A., Rosebrock, A.P., Munro, M., Canny, M.D., et al. (2013). A cell cycle-dependent regulatory circuit composed of 53BP1-RIF1 and BRCA1-CtIP controls DNA repair pathway choice. Mol. Cell *49*, 872–883.

Falck, J., Forment, J.V., Coates, J., Mistrik, M., Lukas, J., Bartek, J., and Jackson, S.P. (2012). CDK targeting of NBS1 promotes DNA-end resection, replication restart and homologous recombination. EMBO Rep. *13*, 561–568.

Feng, L., Fong, K.W., Wang, J., Wang, W., and Chen, J. (2013). RIF1 counteracts BRCA1-mediated end resection during DNA repair. J. Biol. Chem. *288*, 11135–11143.

Findlay, S., Heath, J., Luo, V.M., Malina, A., Morin, T., Coulombe, Y., Djerir, B., Li, Z., Samiei, A., Simo-Cheyou, E., et al. (2018). SHLD2/FAM35A co-operates with REV7 to coordinate DNA double-strand break repair pathway choice. EMBO J. *37*, e100158.

Frank-Vaillant, M., and Marcand, S. (2002). Transient stability of DNA ends allows nonhomologous end joining to precede homologous recombination. Mol. Cell *10*, 1189–1199.

Garzón, J., Ursich, S., Lopes, M., Hiraga, S.I., and Donaldson, A.D. (2019). Human RIF1-protein phosphatase 1 prevents degradation and breakage of nascent DNA on replication stalling. Cell Rep. *27*, 2558–2566.e4.

Ghezraoui, H., Oliveira, C., Becker, J.R., Bilham, K., Moralli, D., Anzilotti, C., Fischer, R., Deobagkar-Lele, M., Sanchiz-Calvo, M., Fueyo-Marcos, E., et al. (2018). 53BP1 cooperation with the REV7-shieldin complex underpins DNA structure-specific NHEJ. Nature *560*, 122–127.

Gunn, A., and Stark, J.M. (2012). I-SceI-based assays to examine distinct repair outcomes of mammalian chromosomal double strand breaks. Methods Mol. Biol. *920*, 379–391.

Gupta, R., Somyajit, K., Narita, T., Maskey, E., Stanlie, A., Kremer, M., Typas, D., Lammers, M., Mailand, N., Nussenzweig, A., et al. (2018). DNA repair network analysis reveals shieldin as a key regulator of NHEJ and PARP inhibitor sensitivity. Cell *173*, 972–988.e23.

Hiraga, S., Alvino, G.M., Chang, F., Lian, H.Y., Sridhar, A., Kubota, T., Brewer, B.J., Weinreich, M., Raghuraman, M.K., and Donaldson, A.D. (2014). Rif1 controls DNA replication by directing protein phosphatase 1 to reverse Cdc7-mediated phosphorylation of the MCM complex. Genes Dev. *28*, 372–383.

Hiraga, S.I., Ly, T., Garzón, J., Hořejší, Z., Ohkubo, Y.N., Endo, A., Obuse, C., Boulton, S.J., Lamond, A.I., and Donaldson, A.D. (2017). Human RIF1 and protein phosphatase 1 stimulate DNA replication origin licensing but suppress origin activation. EMBO Rep. *18*, 403–419.

Hoa, N.N., Kobayashi, J., Omura, M., Hirakawa, M., Yang, S.H., Komatsu, K., Paull, T.T., Takeda, S., and Sasanuma, H. (2015). BRCA1 and CtIP are both required to recruit Dna2 at double-strand breaks in homologous recombination. PLoS ONE *10*, e0124495.

Huertas, P., and Jackson, S.P. (2009). Human CtIP mediates cell cycle control of DNA end resection and double strand break repair. J. Biol. Chem. *284*, 9558–9565.

Isobe, S.Y., Nagao, K., Nozaki, N., Kimura, H., and Obuse, C. (2017). Inhibition of RIF1 by SCAI allows BRCA1-mediated repair. Cell Rep. *20*, 297–307.

Isono, M., Niimi, A., Oike, T., Hagiwara, Y., Sato, H., Sekine, R., Yoshida, Y., Isobe, S.Y., Obuse, C., Nishi, R., et al. (2017). BRCA1 directs the repair

pathway to homologous recombination by promoting 53BP1 dephosphorylation. Cell Rep. *18*, 520–532.

Kim, J.S., Krasieva, T.B., Kurumizaka, H., Chen, D.J., Taylor, A.M., and Yokomori, K. (2005). Independent and sequential recruitment of NHEJ and HR factors to DNA damage sites in mammalian cells. J. Cell Biol. *170*, 341–347.

Lord, C.J., and Ashworth, A. (2013). Mechanisms of resistance to therapies targeting BRCA-mutant cancers. Nat. Med. *19*, 1381–1388.

Miki, Y., Swensen, J., Shattuck-Eidens, D., Futreal, P.A., Harshman, K., Tavtigian, S., Liu, Q., Cochran, C., Bennett, L.M., Ding, W., et al. (1994). A strong candidate for the breast and ovarian cancer susceptibility gene BRCA1. Science *266*, 66–71.

Mirman, Z., Lottersberger, F., Takai, H., Kibe, T., Gong, Y., Takai, K., Bianchi, A., Zimmermann, M., Durocher, D., and de Lange, T. (2018). 53BP1-RIF1-shieldin counteracts DSB resection through CST- and Polα-dependent fill-in. Nature *560*, 112–116.

Murakami, K., Günesdogan, U., Zylicz, J.J., Tang, W.W.C., Sengupta, R., Kobayashi, T., Kim, S., Butler, R., Dietmann, S., and Surani, M.A. (2016). NANOG alone induces germ cells in primed epiblast in vitro by activation of enhancers. Nature *529*, 403–407.

Noordermeer, S.M., Adam, S., Setiaputra, D., Barazas, M., Pettitt, S.J., Ling, A.K., Olivieri, M., Álvarez-Quilón, A., Moatti, N., Zimmermann, M., et al. (2018). The shieldin complex mediates 53BP1-dependent DNA repair. Nature *560*, 117–121.

Nozawa, R.S., Nagao, K., Masuda, H.T., Iwasaki, O., Hirota, T., Nozaki, N., Kimura, H., and Obuse, C. (2010). Human POGZ modulates dissociation of HP1α from mitotic chromosome arms through Aurora B activation. Nat. Cell Biol. *12*, 719–727.

Nozawa, R.S., Nagao, K., Igami, K.T., Shibata, S., Shirai, N., Nozaki, N., Sado, T., Kimura, H., and Obuse, C. (2013). Human inactive X chromosome is compacted through a PRC2-independent SMCHD1-HBiX1 pathway. Nat. Struct. Mol. Biol. *20*, 566–573.

Peti, W., Nairn, A.C., and Page, R. (2013). Structural basis for protein phosphatase 1 regulation and specificity. FEBS J. *280*, 596–611.

Reginato, G., and Cejka, P. (2020). The MRE11 complex: A versatile toolkit for the repair of broken DNA. DNA Repair (Amst.) *91-92*, 102869.

Roy, R., Chun, J., and Powell, S.N. (2011). BRCA1 and BRCA2: different roles in a common pathway of genome protection. Nat. Rev. Cancer *12*, 68–78.

Sartori, A.A., Lukas, C., Coates, J., Mistrik, M., Fu, S., Bartek, J., Baer, R., Lukas, J., and Jackson, S.P. (2007). Human CtIP promotes DNA end resection. Nature *450*, 509–514.

Setiaputra, D., and Durocher, D. (2019). Shieldin—The protector of DNA ends. EMBO Rep. *20*, e47560.

Shibata, A., and Jeggo, P.A. (2020). Roles for the DNA-PK complex and 53BP1 in protecting ends from resection during DNA double-strand break repair. J. Radiat. Res. (Tokyo) *61*, 718–726.

Shibata, A., Conrad, S., Birraux, J., Geuting, V., Barton, O., Ismail, A., Kakarougkas, A., Meek, K., Taucher-Scholz, G., Löbrich, M., and Jeggo, P.A. (2011). Factors determining DNA double-strand break repair pathway choice in G2 phase. EMBO J. *30*, 1079–1092.

Sukackaite, R., Cornacchia, D., Jensen, M.R., Mas, P.J., Blackledge, M., Enervald, E., Duan, G., Auchynnikava, T., Köhn, M., Hart, D.J., and Buonomo, S.B.C. (2017). Mouse Rif1 is a regulatory subunit of protein phosphatase 1 (PP1). Sci. Rep. *7*, 2119.

Symington, L.S., and Gautier, J. (2011). Double-strand break end resection and repair pathway choice. Annu. Rev. Genet. *45*, 247–271.

Tachiwana, H., Shimura, M., Nakai-Murakami, C., Tokunaga, K., Takizawa, Y., Sata, T., Kurumizaka, H., and Ishizaka, Y. (2006). HIV-1 Vpr induces DNA double-strand breaks. Cancer Res. *66*, 627–631.

Takeda, S., Hoa, N.N., and Sasanuma, H. (2016). The role of the Mre11-Rad50-Nbs1 complex in double-strand break repair-facts and myths. J. Radiat. Res. (Tokyo) *57* (*Suppl 1*), i25–i32.

Tomida, J., Takata, K.I., Bhetawal, S., Person, M.D., Chao, H.P., Tang, D.G., and Wood, R.D. (2018). FAM35A associates with REV7 and modulates DNA damage responses of normal and BRCA1-defective cells. EMBO J. *37*, e99543.

Trinkle-Mulcahy, L., Andersen, J., Lam, Y.W., Moorhead, G., Mann, M., and Lamond, A.I. (2006). Repo-Man recruits PP1γ to chromatin and is essential for cell viability. J. Cell Biol. *172*, 679–692.

Wang, H., Shi, L.Z., Wong, C.C., Han, X., Hwang, P.Y., Truong, L.N., Zhu, Q., Shao, Z., Chen, D.J., Berns, M.W., et al. (2013). The interaction of CtIP and Nbs1 connects CDK and ATM to regulate HR-mediated double-strand break repair. PLoS Genet. *9*, e1003277.

Xu, G., Chapman, J.R., Brandsma, I., Yuan, J., Mistrik, M., Bouwman, P., Bartkova, J., Gogola, E., Warmerdam, D., Barazas, M., et al. (2015). REV7 counteracts DNA double-strand break resection and affects PARP inhibition. Nature *521*, 541–544.

Zhu, S., Fisher, L.A., Bessho, T., and Peng, A. (2017). Protein phosphatase 1 and phosphatase 1 nuclear targeting subunit-dependent regulation of DNA-dependent protein kinase and non-homologous end joining. Nucleic Acids Res. *45*, 10583–10594.

Zimmermann, M., and de Lange, T. (2014). 53BP1: Pro choice in DNA repair. Trends Cell Biol. *24*, 108–117.

Zimmermann, M., Lottersberger, F., Buonomo, S.B., Sfeir, A., and de Lange, T. (2013). 53BP1 regulates DSB repair using Rif1 to control 5′ end resection. Science *339*, 700–704.

STAR★METHODS

KEY RESOURCES TABLE

REAGENT or RESOURCE	SOURCE	IDENTIFIER
Antibodies		
Goat polyclonal anti-RIF1 (clone N-20)	Santa Cruz	Cat# sc-55979; RRID: AB_2126818
Rabbit polyclonal anti-RIF1	Bethyl	Cat# A300-569A; RRID: AB_669804
Mouse monoclonal anti-PP1 (clone E-9)	Santa Cruz	Cat# sc-7482 RRID: AB_628177
Goat polyclonal anti-PP1α (clone C-19)	Santa Cruz	Cat# sc-6104 RRID: AB_2299993
Mouse monoclonal anti-CtIP (clone 14-1)	Active Motif	Cat# 61141 RRID: AB_2714164
Mouse monoclonal anti-γH2AX (clone JBW301)	Merck Millipore	Cat# 05-636 RRID: AB_309864
Rabbit monoclonal anti-γH2AX Antibody (clone 20E3)	CST	Cat# 9718 RRID: AB_2118009
Rabbit monoclonal anti-REV7 (clone EPR13657)	Abcam	Cat# ab180579 RRID: AB_2890174
Rabbit polyclonal anti-BRCA1	Merck Millipore	Cat# 07-434 RRID: AB_2275035
Rabbit polyclonal anti-53BP1	Novus Biologicals	Cat# NB 100-304 RRID: AB_350221
Rabbit polyclonal anti-NBS1	Novus Biologicals	Cat# NB 100-143 RRID: AB_350080
Mouse monoclonal anti-RPA2 (clone 9H8)	Abcam	Cat# ab2175 RRID: AB_302873
Rabbit polyclonal anti-RAD51	Tachiwana et al., 2006	N/A
Mouse monoclonal anti-Cyclin A (clone CY-A1)	Merck Millipore	Cat# C4710 RRID: AB_1078603
Mouse monoclonal anti-Tubulin (clone DM1A)	Merck Millipore	Cat# T6199 RRID: AB_477583
Mouse monoclonal anti-FLAG (clone M2)	Merck Millipore	Cat# F1804 RRID: AB_262044
Mouse monoclonal anti-SCAI (clone 17C3)	Isobe et al., 2017	N/A
Donkey polyclonal anti-mouse IgG AlexaFluor 488	Jackson ImmunoResearch	Cat# 715-545-151 RRID: AB_2341099
Goat polyclonal anti-mouse IgG Cy3	Jackson ImmunoResearch	Cat# 115-165-071 RRID: AB_2338687
Goat polyclonal anti-mouse IgG Cy5	Jackson ImmunoResearch	Cat# 115-175-071 RRID: AB_2338711
Goat polyclonal anti-rabbit IgG Cy3	Jackson ImmunoResearch	Cat# 711-165-152 RRID: AB_2307443
Donkey polyclonal anti-goat IgG AlexaFluor 647	Jackson ImmunoResearch	Cat# 705-606-147 RRID: AB_2340438
Goat polyclonal anti-mouse IgG HRP	BIORAD	Cat# 172-1011 RRID: AB_11125936
Goat polyclonal anti-rabbit IgG HRP	BIORAD	Cat# 170-6515 RRID: AB_11125142
Bovine polyclonal anti-goat IgG HRP	Santa Cruz	Cat# sc-2378 RRID: AB_634813
Duolink™ *In Situ* PLA® Probe Anti-Mouse PLUS	Sigma-Aldrich	Cat# DUO92001 RRID: AB_2810939
Duolink™ *In Situ* PLA® Probe Anti-Rabbit MINUS	Sigma-Aldrich	Cat# DUO92005 RRID: AB_2810942
Chemicals, peptides, and recombinant proteins		
Hoechst (bisbenzimide H 33342 trihydrochloride)	Sigma-Aldrich	Cat# B2261
ProLong Gold antifade reagent	Thermo Fisher	Cat# P36930
Paraformaldehyde 16% Solution, EM Grade	Electron Microscopy Sciences	Cat# 15710-S
Anti-FLAG M2 Affinity Gel	Sigma-Aldrich	Cat# A2220
Duolink™ *In Situ* Mounting Medium with DAPI	Sigma-Aldrich	Cat# DUO82040

(*Continued on next page*)

Continued

REAGENT or RESOURCE	SOURCE	IDENTIFIER
Doxycycline hyclate	Sigma-Aldrich	Cat# D9891
MRE11 inhibitor Mirin	Abcam	Cat# ab141182
PARP inhibitor Olaparib	Selleckchem	Cat# S1060
ATM inhibitor KU55933	Abcam	Cat# ab120637
Neocarzinostatin	Sigma-Aldrich	Cat# N9162
Lipofectamine RNAiMAX	Thermo Fisher	Cat# 133778-150
Lipofectamine 2000	Thermo Fisher	Cat# 11668-019
GeneJuice	Merck Millipore	Cat# 70967-3
ISOGEN	FUJIFILM Wako	Cat# 317-02503
Critical commercial assays		
Click-IT Plus EdU Alexa Fluor 647 Imaging Kit	Thermo Fisher	Cat# C10340
Duolink™ *In Situ* Detection Regents Red	Sigma-Aldrich	Cat# DUO92008
TAKARA RNA PCR Kit (AMV) ver.3.0	TAKARA	Cat# RR019A
TB Green Premix Ex TaqII	TAKARA	Cat# RR820A
Experimental models: Cell lines		
HeLa, wild-type	Nozawa et al., 2010	N/A
HeLa: RIF1 K/O; RIF1 knockout cell line	This paper	N/A
HeLa: K/O+RIF1WT	This paper	N/A
HeLa: K/O+RIF1ppC	This paper	N/A
U2OS EJ5-GFP	Gift from Jeremy M. Stark, described in Gunn and Stark (2012)	N/A
U2OS DR-GFP	Gift from Jeremy M. Stark, described in Gunn and Stark (2012)	N/A
Flp-In T-REx 293	Thermo Fisher	Cat# R78007
HeLa: GFP-PP1α	This paper	N/A
Oligonucleotides		
RIF1 siRNA	Dharmacon	Cat# D-027983-02
RIF1 siRNA (siRIF1-2)	Thermo Fisher	Cat# HSS124071
REV7 siRNA	Thermo Fisher	Cat# s20466
SHLD2 siRNA	Thermo Fisher	Cat# HSS147691
53BP1 siRNA	Thermo Fisher	Cat# HSS110909
SCAI siRNA	Thermo Fisher	Cat# HSS138873
BRCA1 siRNA	Thermo Fisher	Cat# HSS186097
Control siRNA: Sense, 5′-GUACCGCACGUCAUUCGUAUC-3′	Nozawa et al., 2010	N/A
Control siRNA: Anti-sense, 5′-UACGAAUGACGUGCGGUACGU-3′	Nozawa et al., 2010	N/A
sgRNA targeting human RIF1 locus: 5′-AAGTCTCCAACAGCGGCGCG-3′	This paper	N/A
Primers for RT-qPCR for human SHLD2: Forward, 5′-CCACGCAGTACTAAGAGTTG-3′	This paper	N/A
Primers for RT-qPCR for human SHLD2: Reverse, 5′-GGCCTGTTCCACTGTT AAC-3′	This paper	N/A
Primers for RT-qPCR for human GAPDH: Forward, 5′-CTCTCCAGAACATCAT CCC-3′	This paper	N/A

(*Continued on next page*)

Continued

REAGENT or RESOURCE	SOURCE	IDENTIFIER
Primers for RT-qPCR for human GAPDH: Reverse, 5′-CTAGACGGCAGGTCAG GTC-3′	This paper	N/A
Recombinant DNA		
Plasmid: px330-U6-Chimeric_BB-CBh-hSpCas9	Addgene	Cat# 42230
Plasmid: pPyCAG-monomeric Kusabira Orange-IRES-Pac	Gift from Kazuhiro Murakami, described in Murakami et al. (2016)	N/A
Plasmid: PiggyBac-based doxycycline (Dox)-inducible (pPBhCMV1) vector	Gift from Kazuhiro Murakami, described in Murakami et al. (2016)	N/A
Plasmid: pPBCAG-rtTA-IRES-Neor	Gift from Kazuhiro Murakami, described in Murakami et al. (2016)	N/A
Plasmid: pmPB, encoding PiggyBac transposase vector	Gift from Hiroshi Kimura	N/A
Plasmid: pcDNA/TO-FLAG vector	Nozawa et al., 2010	N/A
Plasmid: pcDNA/TO-FLAG-RIF1WT	This paper	N/A
Plasmid: pcDNA/TO-FLAG-RIF1ppN	This paper	N/A
Plasmid: pcDNA/TO-FLAG-RIF1ppC	This paper	N/A
Plasmid: pcDNA/TO-FLAG-RIF1pp	This paper	N/A
Plasmid: pPBhCMV1-FLAG-sfGFP vector	This paper	N/A
Plasmid: pPBhCMV1-FLAG-sfGFP-RIF1WT (siRNA-resistant)	This paper	N/A
Plasmid: pPBhCMV1-FLAG-sfGFP-RIF1 ppC (siRNA-resistant)	This paper	N/A
Plasmid: pPBhCMV1-FLAG-mCherry vector	This paper	N/A
Plasmid: pPBhCMV1-FLAG-mCherry-RIF1 WT (siRNA-resistant)	This paper	N/A
Plasmid: pPBhCMV1-FLAG-mCherry-RIF1 ppC (siRNA-resistant)	This paper	N/A
Plasmid: pcDNA3.1-GFP-PP1α	This paper	N/A
Plasmid: pCBASce (I-SceI expression vector)	Gift from Jeremy M. Stark, described in Gunn and Stark (2012)	N/A
Software and algorithms		
NIS-Elements ver5.20	Nikon	https://www.microscope.healthcare.nikon.com/products/software/nis-elements
R ver3.6.1	The R Foundation for Statistical Computing	http://www.R-project.org
ImageJ 1.42q	NIH	https://imagej.nih.gov/ij/
Mascot ver2.3.02	MATRIX SCIENCE	https://www.matrixscience.com/

RESOURCE AVAILABILITY

Lead contact

Further information and requests for resources and reagents should be directed to and will be fulfilled by the lead contact, Chikashi Obuse (obuse@bio.sci.osaka-u.ac.jp).

Materials availability

All unique regents generated in this study are available from the lead contact upon request.

Data and code availability

This study did not generate any unique datasets or code.

EXPERIMENTAL MODEL AND SUBJECT DETAILS

Flp-In-T-REx 293 (Life Technologies), HeLa, and their derivatives were grown in D-MEM (nacalai tesque) supplemented with 5% Fetal Bovine Serum (FBS, Life Technologies) and 100 μg/ml of penicillin and 100 unit/ml of streptomycin (Life Technologies) in 5% CO2 at 37°C. For U2OS EJ5-GFP and U2OS DR-GFP, the same medium supplemented with 10% FBS was used.

METHOD DETAILS

Drug treatment

Doxycycline (Dox, Sigma-Aldrich) was added to cell culture at 1 μg/ml 24h before irradiation. Mirin (MRE11 exonuclease inhibitor, Abcam) was added to cell culture at 100 μM 10 min before irradiation. KU55933 (ATM inhibitor, Abcam) was added to cell culture at 10 μM 10 min before the addition of Neocarzinostatin. Neocarzinostatin (Sigma-Aldrich) was added to cell culture at 150 ng/ml.

RNA interference

RNA interference (RNAi) was performed as described (Nozawa et al., 2010). Briefly, cells were transfected with 20 nM siRNAs using Lipofectamine RNAiMAX (Thermo Fisher). Oligonucleotides (Supplier, identification numbers) used for RNAi in this study are as follows: RIF1 (Dharmacon, #D-027983-02), RIF1-2 (Thermo Fisher, # HSS124071), REV7 (Thermo Fisher, #s20466), SHLD2 (Thermo Fisher, #HSS147691), 53BP1 (Thermo Fisher, # HSS110909), SCAI (Thermo Fisher, # HSS138873), BRCA1 (Thermo Fisher, # HSS186097). Oligonucleotides used for control siRNA: (sense); 5′-GUACCGCACGUCAUUCGUAUC-3′ and (anti-sense); 5′-UAC GAAUGACGUGCGGUACGU-3′ (Nozawa et al., 2010).

Antibodies

For primary antibody (host animal, supplier, identification clone name and dilution with applications) used in this study are as follows: anti-RIF1 (goat; sc-55979; Santa Cruz; 1:300 for western blotting (WB) and 1:500 for immunofluorescence (IF)), anti-RIF1 (rabbit; A300-569A; Bethyl; 1:500 for WB), PP1 (mouse; sc-7482; Santa Cruz; 1:500 for WB), anti-PP1α (goat; sc-6104; Santa Cruz; 1:500 for IF), CtIP (mouse; 14-1; Active Motif, 1:500 for WB, 1:300 for IF), anti-γH2AX (mouse; JBW301, Millipore, 1:5000 for IF), anti-γH2AX (rabbit; 20E3, CST, 1:500 for IF), anti-REV7 (rabbit; EPR13657; abcam; 1:500 for WB), anti-RAD51 (rabbit polyclonal antibody; a gift from Hitoshi Kurumizaka; 1:3000 for IF) (Tachiwana et al., 2006), anti-53BP1 (rabbit; NB 100-304; Novus Biologicals; 1:1000 for WB and 1:5000 for IF), anti-SCAI (mouse; 17C3; described previously; hybridoma culture supernatants were used at 1:100 for WB) (Isobe et al., 2017), anti-BRCA1 (rabbit; 07-434; Millipore; 1:500 for WB), anti-NBS1 (rabbit; NB 100-143; Novus Biologicals; 1:500 for IF), anti-RPA2 (mouse; 9H8; abcam; 1:300 for IF), anti-cyclin A (mouse; CY-A1; Sigma; 1:1000 for IF), anti-Tubulin (mouse; DM1A; Sigma; 1:10000 for WB), anti-FLAG (mouse; M2; Sigma; 1:1000 for WB). Secondary antibodies (KEY RESOURCES TABLE) were used at 1:10000 dilution for western blot, and at 1:500 dilution for immunofluorescence.

Plasmid construction

siRNA-resistant RIF1 silent mutation was generated as that the siRNA target: 5′-AGACGGTGCTCTATTGTTA-3′ was replaced with 5′-cGtaGaTGtTCaATaGTac-3′. cDNA encoding PP1α was cloned from HeLa mRNA by RT-PCR. RIF1 derivatives were generated from plasmids described in Hiraga et al. (2017). All sequences obtained by PCR were verified by nucleotide sequencing. Detailed information about plasmid constructions described in this paper is available on request.

Plasmid transfection and establishment of cell lines

Plasmid transfections were performed by the manufacturer's procedures. Lipofectamine 2000 (Thermo Fisher) was used for immunoprecipitation experiments and Gene Juice (Millipore) for the establishment of the cell lines.

For establishment of RIF1 knock out HeLa cell (RIF1 K/O), pX330 harboring a guide RNA for RIF1 (See Key resource table) and pPyCAG-monomeric Kusabira Orange-IRES-Pac (for puromycin selection) were co-transfected into HeLa cells. Puromycin resistant cells were re-plated and isolated as single clones. RIF1 gene disruption was confirmed by direct-sequencing and western blotting analysis.

For establishment of RIF1 K/O cell lines with Dox-inducible RIF1 derivatives (WT^{KI} and ppC^{KI}), RIF1 K/O cells were transfected with pPBhCMV1 harboring FLAG-sfGFP-tagged RIF1WT or RIF1ppC under the control of doxycycline promoter, pPBCAG-rtTA-IRES-Neor (for expression of reverse tetR with the C-terminal domain of VP16), and pmPB (for expression of PiggyBac transposase). G418 resistant clones were isolated. For establishment of HeLa cell line expressing GFP-PP1α, cells were transfected with pcDNA3.1-based GFP-PP1α expression vector and G418 resistant clones were isolated.

Immunofluorescence and microscopy

Immunofluorescence microscopy was performed essentially as described (Nozawa et al., 2013). Cells were grown on glass coverslips for X-ray irradiation (MX-80 Labo; mediXtech Japan, 1.1 Gy/min). All the cases other than visualizing CtIP, RPA2, and γH2AX, cells were fixed with −20°C methanol for 5 min and then re-fixed with 3% formaldehyde in 250mM HEPES pH 7.4 at R.T. for 10 min. For visualization of CtIP or RPA2, cells were fixed with 3% formaldehyde in 250mM HEPES pH 7.4 containing 0.5% Triton X-100 on

ice for 0.5 h. For γH2AX, fixation was essentially performed as that for CtIP and RPA2 without 0.5% Triton X-100. Fixed cells were permeabilized with 0.5% Triton X-100 on ice for 5 min, and blocked with 0.1% BSA in PBS on ice for 20 min. After that cells were incubated with primary antibodies at R.T. for 1 hour, followed by incubation with fluorochrome-conjugated secondary antibodies along with Hoechst for 30 min. Coverslips were finally mounted ProLong Gold (Thermo Fisher). If assignment of S/G2 or G2 cells was indicated, cells were co-stained with cyclin A, or treated with 10 μM EdU for 10min before fixation, respectively. EdU click-iT chemistry was performed as manufacturer's instructions (Thermo Fisher). Cell images were essentially captured using a confocal laser microscope (C2 system connected to a Ti-E inverted microscope; Nikon). For BRCA1 IRIF and NBS1 visualizations, cell images were captured using a Andor Zyla 5.5 cCMOS camera connected to a microscope (Ti-E inverted microscope; Nikon). To count all foci in a nucleus, five z axis with 0.4-μm interval images were stacked. The number of the nuclear focus signals was automatically counted using Nis-Elements software version 5.20 (Nikon) (Isobe et al., 2017).

Proximity ligation assay (PLA)

Proximity ligation assay was performed basically as for the immunofluorescence procedure up to the primary antibody treatment (see details above) and then treated with PLA-probe-conjugated secondary antibodies, followed by ligation and amplification steps according to the manufacturer's protocol (Duolink *in situ* proximity ligation assay, Sigma-Aldrich). Signals were captured by confocal laser microscope and the number of the nuclear focus signals counted (see above in Method details).

Western blotting and immunoprecipitation

Protein extraction, immunoprecipitation and western blotting were performed as described (Nozawa et al., 2010). For whole cell protein extraction, cells were lysed in SDS buffer (62.5 mM Tris-HCl pH6.8, 1% SDS, 10% glycerol, 0.625% 2-Mercaptoethanol). The extracts from 1.0 × 10^5 cells were separated by precast gels (FUJIFILM Wako) for Figures 1B, S1B, S3, S4A, and S5A or house-made gels for Figure 3B and S2B. Transfer of proteins onto PVDF membranes and incubation with primary/secondary antibodies were performed by standard procedures. The blots probed with secondary antibodies conjugated with horse radish peroxidase were exposed with ImmunoStar (FUJIFILM Wako) and imaged with LumiVision PRO 400EX system (AISIN) or LuminoGraph I system (ATTO). Quantifications of bands intensity were done by ImageJ (Figure S4A).

For immunoprecipitation, cells were lysis with CSK buffer (0.5 M NaCl, 0.1% Triton X-100, 10 mM PIPES-NaOH pH 7.0, 300 mM sucrose, 1 mM $MgCl_2$, 1 mM EDTA) supplemented with 100 μM PMSF (phenylmethanesulfonylfluoride) and 2 μg/ml leupeptin, and centrifugated supernatant was used as nuclear extract. Anti-FLAG M2 Affinity Gel (Sigma-Aldrich) was used for immunoprecipitation of FLAG-tagged RIF1 complexes from the nuclear extracts.

Mass spectrometry analysis

Proteomic analysis using mass spectrometry was performed as described (Nozawa et al., 2010). Briefly, samples were separated by 12.5% gel of SDS–PAGE, and each lane was cut into nine pieces for trypsinization for liquid chromatography coupled to tandem MS (LC/MS/MS). The raw data files were searched against the international protein index human database (version 3.63) including with Mascot software (Matrix Science). The number of unique spectra and the percent coverage were computed from data summarizing two measurements from all pieces of a gel and identified for each protein was converted to emPAI (exponentially modified protein abundance index) values. Specific peptides for PP1α, PP1β and PP1γ were detected, respectively. Common peptides among the subtypes were assigned to the all subtypes, respectively. When no spectrum was identified, the number of unique spectra was considered as 0.8 to avoid underestimation because of the detection limit.

Quantitative real-time PCR

To evaluate the efficiency of SHLD2 knockdown, we used quantitative PCR analysis. Total RNA from siRNA-treated HeLa cells was extracted using ISOGEN (FUJIFILM Wako), according to the manufacturer's protocol. The total RNA was reverse transcribed using the TaKaRa RNA PCR Kit (AMV) ver.3.0. Quantitative real-time PCR was performed according to standard procedures using TB Green Premix Ex TaqII (TaKaRa) and Mx3000P (STRATAGENE). Primer sets: SHLD2 (5′– ccacgcagtactaagagttg–3′ and 5′– ggc ctgttccactgttaac–3′), GAPDH (5′– ctctccagaacatcatccc–3′ and 5′– ctagacggcaggtcaggtc–3′)

Colony formation assay

For colony formation assay, following steps were performed. Doxycycline was added 24 hours after transfection with siRNA (control or BRCA1), and then after 24 hours, 500-1000 cells were plated in each well of a 6-well plate. Olaparib (Selleckchem) was added at the indicated doses 8 h after the plating. After 72 hr incubation, Olaparib and Doxycycline were washed out and replaced with fresh medium. One week later, the colonies were fixed with methanol at −20°C for 5 min and stained with Giemsa solution. Colonies were counted and the surviving rates were calculated as ratios to the number of those without Olaparib.

DSB reporter assay

A DSB reporter assays using U2OS EJ5-GFP (for NHEJ) or U2OS DR-GFP (for HR) were performed essentially as described (Gunn and Stark, 2012; Isobe et al., 2017). 24 h after siRNA transfection by RNAiMAX (Life Technologies), cells were transfer to new well with dilution. After subsequent 24 h, cells were transfected with siRNA, plasmid for I-SceI expression, and plasmids for mCherry expression or

mCherry-tagged siRNA-resistant RIF1 derivatives by Lipofectamine 2000 (Life Technologies). Then, after 72 h incubation, GFP- and mCherry-positive cells were counted by flow cytometry (Cell Sorter SH800S; Sony).

QUANTIFICATION AND STATISTICAL ANALYSIS

For bee swarm plot, statistical significance was determined by Mann-Whitney U-test using R software "*," "**," and "***" means p value < 0.001. The number of experimental replicates is stated as "n" in the figure legend. Error bars represent standard deviation between the experiments analyzed with R software, as indicated in the legends.